Contents lists available at GrowingScience

Engineering Solid Mechanics

homepage: www.GrowingScience.com/esm

Prediction of threshold von-mises stress distribution of the sections of oil pipeline steel with internal corrosion defects using finite element analysis

Sergei Sherbakov[a], Daria Podgayskaya[a], Pawan Kumar[a*], Pavel Poliakov[b] and Vasilii Dobrianskii[b]

[a]*Joint institute of mechanical engineering of the National Academy of Sciences of Belarus, 220012 Minsk, Belarus*
[b]*Moscow Aviation Institute (National Research University), 125993 Moscow, Russia*

ARTICLEINFO

Article history:
Received 18 July 2024
Accepted 26 January 2025
Available online
26 January 2025

Keywords:
Structural steel pipe
Von-Mises stress
Finite element analysis
Stress intensity
Failure pressure

ABSTRACT

The current work presents a finite element analysis (FEA) based investigation of the structural steel pipe with internal corrosion defects. A total of 27 different geometrical conditions for internal corrosion defect were considered using 3 different internal pressures of 2.2 MPa, 4.5 MPa, and 6 MPa. The validation of the FEA model was carried out using the analytical solution for failure pressure using radial and hoop stresses. The failure pressure of the uncorroded pipe was 11.5 MPa. In contrast, for pipe with internal corrosion defect having the largest defect (1.7 mm), largest length (454 mm), and sharpest geometry (width of 30 mm), the failure pressure from FEA was 6 MPa. The remaining strength at this boundary condition was 0.521. The radial stress influences the strain in wall thickness which was 8.8 mm and much less as compared to other dimensions of pipeline which diminishes the material's ability to resist the failure pressure. The Von-Mises stress accumulation inside the interface increases the stress intensity (K) distribution at the vicinity of the internal corrosion defect geometry vis-à-vis lowers the K-distribution just outside of the internal corrosion defect. The largest factor of safety (FOS) of 2.11 was obtained at threshold boundary conditions considering fatigue limit as the optimum stress. It is then suggested that the FOS for the "break-before-leak" leak model can be anywhere between 2.11 to 1.45 and hence the pipeline cannot burst into rapture.

1. Introduction

The steel pipelines carriage crude oil to refineries and processing plants where they undergo distillation and other production processes (Alobaidi et al., 2015; Bagheri et al., 2013; Ijaola et al., 2020; Ilman, 2014; Poletskov et al., 2019; Stalheim, 2005). It is understood that most pipelines have been buried underground. Therefore, these pipelines are subjected to both external and internal corrosion (Dugstad et al., 1994; Lopez et al., 2015; Melchers, 2023; Z. Wang et al., 2020). The fluid characteristics have been changed during service time and the pipeline system becomes less responsive to established corrosion mitigation theories (Benamor et al., 2018; Hu & Cheng, 2016; Li et al., 2016; Russell et al., 1959; Z. M. Wang & Zhang, 2016). Internal corrosion (IC) of pipelines is not static and depends on the composition of the material, working temperature, operating pressure, and the flow regime of the transported fluids (Dao et al., 2023). Crude oil contains various impurity products such as CO2, H_2S, O_2, free water, and inherently corrosive bacteria, and the rate of corrosion is a function of concentrations of these impurity products (Godefroid et al., 2017; Hernandez-Rodriguez et al., 2007). As per the US Office of Pipeline Safety, 2002; the percentage of pipeline failure attributed to internal corrosion was 17.24 and the cost of damage occurring was 15.23. Hence, the study of internal corrosion is important for pipeline steels. The pipelines are made of carbon steel as per American Petroleum Institute API 5L steel specifications (Godefroid et al., 2017; Moraes et al., 2021). There are different API grades like X52, X56, X60, X65, and X70 (Race et al., 2020). Here, the preceding of X denotes yield strength in units of ksi. The pipelines of various strengths have been developed to maintain strength to weight ratio. However, the chemistry of these various grades does not change significantly. Hence, all these API grades of the pipeline have similar corrosion behaviour in the oil and gas sector. Subsequently, there is another pipeline steel having higher yield strength (API 5L X80) containing microalloying elements, if we look at the composition of these grades, there is hardly a significant weight % increase in elements like Cr which offers passivation. Consequently, the corrosion behaviour of all these pipeline steels is very much identical. The modelling of internal corrosion has a wide range from industries to laboratories (Capula Colindres et al., 2020; Gartland et al., 2003; Ossai et al., 2016b, 2016a). Modelling can provide an important tool in deciding for designing, operating, and controlling pipeline engineering. Most of the model involves mathematical expression, however,

* Corresponding author.
E-mail addresses: kumarpawan@mail.ru (P. Kumar)

ISSN 2291-8752 (Online) - ISSN 2291-8744 (Print)

doi: 10.5267/j.esm.2025.2.001

qualitative, and physio-chemical models are more explanatory (Vanaei et al., 2017; Vishnuvardhan et al., 2023). There are different models have been developed so far; mechanistic models define the mechanism of inherent reactions having strong theoretical circumstances (Qin & Cheng, 2021). Most of the constants in mechanistic models have an obvious physical meaning. However, semi-empirical models are partially established on theoretical hypotheses (Budhe et al., 2020; Y. Yang et al., 2022). It is an extension/modification of a phenomenon where a relatively inadequate theoretical understanding has been accessible. The supplementary phenomenon is designated with empirical functions. However, empirical models contain very limited non-theoretical background and the constants involved generally have no physical meaning. Constants in empirical models worked as best-fit parameters. It required a large set of databases for validation and acquisition. Most of these models are vast in considering complex internal corrosion defects (IC-defects) considering geometries, difficult to accommodate real-time process parameters, and sometimes require complex numerical integration. In that case, finite element analysis (FEA) based models can provide a real-time solution by considering real-time process parameters associated with IC defects like pressure difference, temperature, and depth of internal corrosion; FEA models can also consider interactions between the internal corrosion defect to a real-time intra-separation distance (Arumugam et al., 2020; Han et al., 2016; J. Sun & Cheng, 2018; Xu & Cheng, 2017; Zhou et al., 2022). However, three-dimensional modelling using FEA requires a more comprehensive analysis of process parameters, and a large number of data sets, and involves multiple physical variables into consideration. It is felt that more comprehensive studies are required to provide solutions to internal corrosion defects in oil pipelines considering different stresses and stress intensity.

Therefore, in the present work, a large number of data sets (81 in numbers) have been generated for the three-dimensional modelling of internal corrosion defects using FEA. The validation of the FEA model was made using the analytical solution for burst pressure at optimum process parameters and radial and hoop stresses. The model further investigates threshold boundary conditions considering leak before break and break before leak hypothesis. The relationship between Von-Mises stresses and stress intensity has also been studied.

2. Materials and Methods

The material under investigation was a structural steel pipe; the mechanical and thermal properties of the material are presented in **Table 1**. The specimen under consideration had a three-dimensional curvilinear geometry having symmetry in the longitudinal direction as shown in **Fig. 1**.

Table 1. Properties of structural steel.

Material	Young's modulus (MPa)	Poisson's ration	Bulk modulus (MPa)	Shear modulus (MPa)	Coefficient of thermal expansion (/ºC)	Compressive yield strength (MPa)	Specific heat constant pressure (MJ/KgºC)
structural steel	2.00E+05	3.00E-01	1.66E+05	7.69E+04	1.20E-05	2.50E+02	4.34E+05

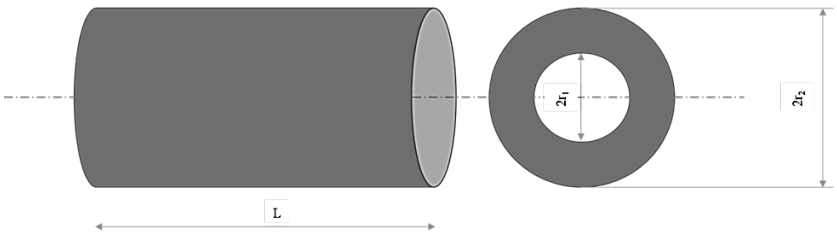

Fig. 1. Symmetry conditions in the longitudinal direction for pipeline steel

The internal radius (r_1), external radius (r_2), and length of pipe (L) were 351.2 mm, 360 mm, and 1500 mm, respectively. The wall thickness of the pipe specimen was 8.8 mm. The effect of internal corrosion was studied by inducing a quarter-elliptical internal defect in the pipe specimen using ANSYS 2022 R1 software. The dimensions of the internal corrosion defect varied in length (z), width (x), and depth (y), their representation in Cartesian coordinates is shown in **Fig. 2**. The corresponding normalized depth (ratio of the depth of defect to the thickness of pipe specimen), elements, and nodes are presented in **Table 2**.

A total of 27 different geometrical conditions for internal corrosion defect were considered by FEA modelling using 3 different internal pressures (p_i) of 2.2 MPa, 4.5 MPa, and 6 MPa. Hence, a total of 81 different states of internal corrosion defect were studied. One-quarter of the section of pipe was considered for FEA modelling using the symmetry of the pipeline geometry.

The external pressure ($p_{ext.}$), temperature gradient (ΔT) and shear stress (τ) were considered null for the current experimental condition. An FEA simulation was done for each internal defect condition and corresponding Von-Mises stress (σ_{mises}), stress intensity (K), principal stress (σ_P), Von-Mises strain (ϵ_{mises}), and principal strain (ϵ_P) were calculated. The validation of the FEA model was done using the analytical solution for radial stress (σ_r) and hoop stress ($\sigma_\emptyset$); the validation

also considers failure pressure ($P_{faliure}$) of pipe with internal corrosion defect was done using a modified ASME B13G method (Han et al., 2016; Mousavi & Moghaddam, 2020). The analysis of Von-Mises stresses and stress intensity was done using ANSYS 2022 FEA software.

Table 2. Geometrical dimensions of internal corrosion defects with the number of elements and nodes used for FEA modelling

Condition no.	Length (z), mm	Width (x), mm	Depth (y), mm	Depth/thickness	Elements	Nodes
1	30	26	0.5	0.06	174566	331477
2	30	26	0.9	0.10	174650	331560
3	30	26	1.7	0.19	174170	330896
4	30	62.1	0.5	0.06	176731	334784
5	30	62.1	0.9	0.10	176755	334794
6	30	62.1	1.7	0.19	175650	332982
7	30	134	0.5	0.06	181850	342780
8	30	134	0.9	0.10	182484	343601
9	30	134	1.7	0.19	180268	340170
10	157.4	26	0.5	0.06	182184	342711
11	157.4	26	0.9	0.10	180828	341017
12	157.4	26	1.7	0.19	181329	341958
13	157.4	62.1	0.5	0.06	193187	359948
14	157.4	62.1	0.9	0.10	193580	360431
15	157.4	62.1	1.7	0.19	191972	358206
16	157.4	134	0.5	0.06	220586	401499
17	157.4	134	0.9	0.10	218161	397948
18	157.4	134	1.7	0.19	214570	393042
19	454	26	0.5	0.06	195637	363502
20	454	26	0.9	0.10	194678	362114
21	454	26	1.7	0.19	194863	362169
22	454	62.1	0.5	0.06	228032	413510
23	454	62.1	0.9	0.10	227812	413196
24	454	62.1	1.7	0.19	226263	410687
25	454	134	0.5	0.06	309430	538458
26	454	134	0.9	0.10	300829	525576
27	454	134	1.7	0.19	292613	513354

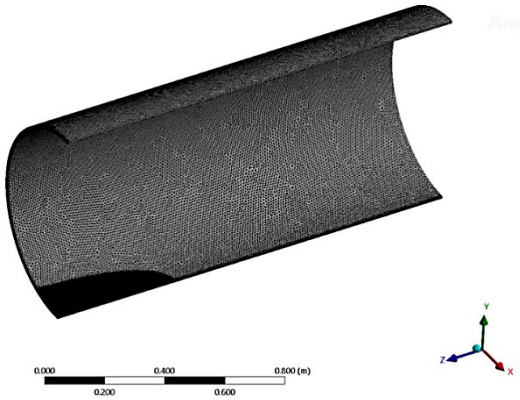

Fig. 2. FEA modelled mesh showing quarter-elliptical internal corrosion defect and corresponding cartesian coordinate system

3. Results and Discussion

This section describes the failure pressure of the pipeline, analytical solutions for radial and hoop stresses, threshold boundary conditions, Von-Mises stresses, stress intensity, and discussion.

3.1. Failure pressure

3.1.1 Failure pressure of uncorroded pipe

The failure pressure (P_{limit}) is the lowest pressure needed to cause irreversible damage to the pipeline by bursting. It is calculated considering zero external pressure and no axial loading (Mousavi & Moghaddam, 2020). The P_{limit} of an uncorroded pipe was calculated using the Von-Mises-based yield criteria (Freire, 2024; M. Sun et al., 2022; Yang, 1980).

$$P_{limit} = \frac{4t}{\left(\sqrt{3}\right)^{n+1}}\left(\frac{\sigma_{uts}}{D_{avg.}}\right) \tag{1}$$

where,
t = thickness of pipeline.
n = strain hardening exponent which is 0.2 for structural steel.
σ_{uts} = ultimate tensile strength of the material.
$D_{avg.}$ = average diameter of the uncorroded pipeline.

The $P_{limit\ (theoretical)}$ was obtained as 11.77 MPa using Eq. (1). This theoretical calculation of P_{limit} was validated by FEA modelling using ANSYS 2022. The hypothesis adopted here was as: at the failure pressure ($P_{limit\ (FEM)}$) the Von-Mises stresses exceed the ultimate tensile strength of the material (σ_{uts}).

The Von-Mises stress distribution and corresponding p_i are presented in Figure 3. It was observed that a maximum Von-Mises stress of 470.67 MPa (greater than $\sigma_{uts} = 460\ MPa$) was obtained at p_i of 11.5 MPa. This stress was greater than σ_{uts} and hence the corresponding p_i provides $P_{limit\ (FEA)}$ for the pipeline. The % error obtained was calculated as:

$$\%\ error = \left|\frac{P_{limit\ (theoretical)} - P_{limit\ (FEA)}}{P_{limit\ (theoretical)}}\right| \times 100 = \left|\frac{11.77-11.50}{11.77}\right| \times 100 = 2.29\%. \quad (2)$$

It is suggested that the above value of % error was in the acceptable range.

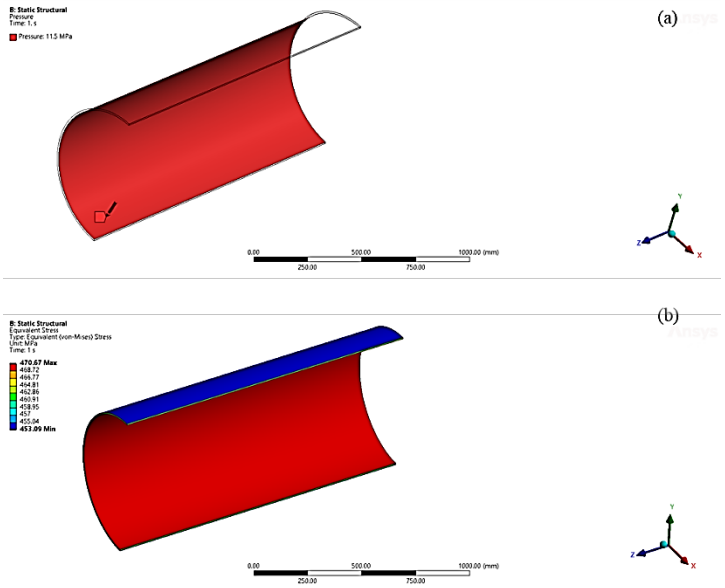

Fig. 3. Uncorroded pipe indicating: (a) applied internal pressure and (b) corresponding Von-Mises stress.

3.1.2 Failure pressure of corroded pipe

For the pipeline with a single internal corrosion defect, the failure pressure($P_{faliure}$) depends upon material properties, the geometry of the defect, and the dimensions of the pipe as (Han et al., 2016; Mousavi & Moghaddam, 2020):

$$P_{faliure} = f(\sigma_{flow}, t, D, d, l, M) \quad (3)$$

where,
σ_{flow} = flow stress of the pipeline material.
t = wall thickness of the pipeline.
D = Outside diameter of the pipeline.
d = depth of internal corrosion defect through the thickness of the pipeline.
l = length of internal corrosion defect.
M = Folias factor. It defines the bulging effect of a shell surface under internal pressure; M is the function of the length of the corrosion defect, the diameter of the pipe, and its thickness (Folias, 1964).

Theoretical assessment of $P_{faliure}$ was done using a modified ASME B13G (Han et al., 2016; Mousavi & Moghaddam, 2020) method as:

$$P_{faliure\ (theoratical)} = \sigma_{flow}\left(\frac{2t}{D}\right)\left(\frac{1-0.85\frac{d}{t}}{1-0.85\frac{1}{M}\frac{d}{t}}\right) \quad (4)$$

The Folias factor was calculated using a non-dimensional parameter z which is also a function of the length of the corrosion defect, the diameter of the pipe, and its thickness. When,

$z = \frac{l^2}{Dt} \leq 50$; Then Folias factor ($M$) was calculated as:

$$M = \sqrt{1 + 0.625(z) + 0.003375(z)^2} \tag{5}$$

However, if

$z > 50$; then M was calculated as:

$$M = 0.032(z) + 3.3 \tag{6}$$

Furthermore, the σ_{flow} was calculated as (Han et al., 2016; Mousavi & Moghaddam, 2020):

$$\sigma_{flow} = \sigma_{ys} + 68.95 \tag{7}$$

The boundary conditions at which the $P_{faliure\ (theoretical)}$ was calculated are presented in **Table 3**.

Table 3. Different boundary conditions as a function of x, y, z, and p_i

BC	Length, z (mm)	Width, x (mm)	Depth, y (mm)	Internal pressure, p_i (MPa)
1	30	134	0.5	2.2
2	30	62.1	0.9	4.5
3	30	26	1.7	6
4	157.4	134	0.5	2.2
5	157.4	62.1	0.9	4.5
6	157.4	26	1.7	6
7	454	134	0.5	2.2
8	454	62.1	0.9	4.5
9	454	26	1.7	6

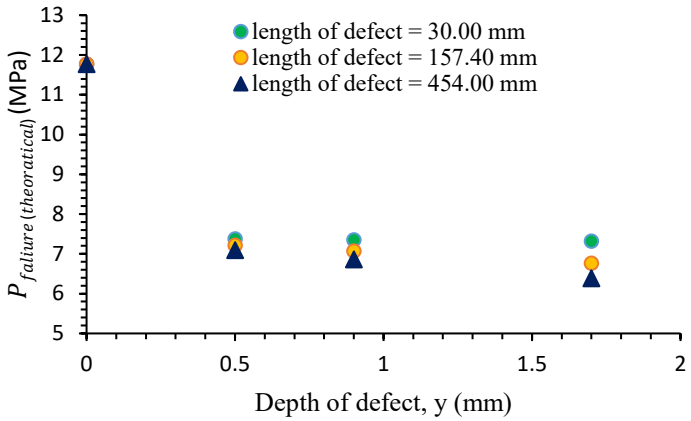

Fig. 4. $P_{faliure\ (theoretical)}$ for internally corroded pipeline for varying "depth" and "length" of defect"

It was observed that the $P_{faliure\ (theoretical)}$ decreases with increasing depth of defect; also, for a given defect depth, the failure pressure decreases with increasing length of defect as shown in Figure 4. Therefore, for the optimum defect geometry (depth of 1.7 mm and length of 454 mmm), the failure pressure was the lowest which is 6.38 MPa. This theoretical calculation of $P_{faliure\ (theoretical)}$ was validated using FEA modelling. The Von-Mises stress for pipes having optimum defect geometry at p_i of 6 MPa is shown in **Fig. 5.**

A maximum Von-Mises stress of 457.1 MPa was obtained by FEA modelling which was nearly equal to σ_{uts}; hence the applied pressure provided the $P_{faliure\ (FEA)}$ which was 6 MPa. The % error was calculated using Eq. (2) as:

$\left|\frac{6.38-6.00}{6.38}\right| \times 100$=5.95%.

The remaining strength (ratio of $P_{faliure\ (FEA)}$ to $P_{limit\ (FEM)}$) at this boundary condition was 0.521. The Von-Mises stress increases for pipes with internal corrosion defects as compared to pipes without defects. It is suggested that this increase in

Von-Mises stress was due to the increase in stress intensity near the vicinity of the defect. Figure 6 shows the $P_{faliure\ (FEA)}$ and stress intensity (K). It was observed that the stresses were accumulated (intensified) at the defect, however, it gradually decreased in the other parts of the specimen. It makes the pipeline susceptible to failure at the defect surface due to a rise in stress intensity vis-à-vis Von-Mises stress.

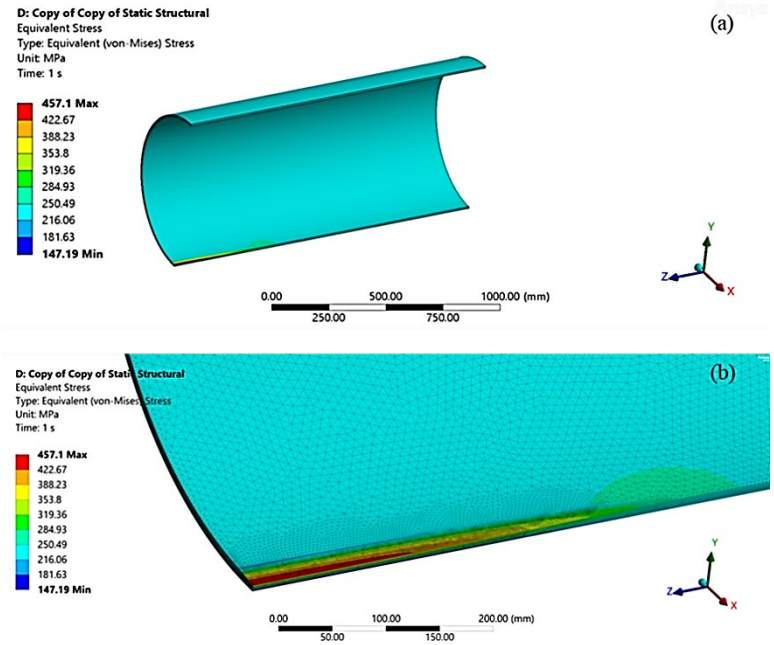

Fig. 5. Von-Mises stresses for pipe specimen having internal corrosion defect depth of 1.7 mm, length of 454 mm, and width of 30 mm. (a) one-quarter geometry (b) localized view at the vicinity of the internal defect.

3.2 Analytical solution for radial and hoop stress

The steel pipeline experiences static and thermal loads due to internal pressure and temperature variations which causes expansion and contraction. Therefore, the stresses in a section of pipe while considering it as an internal system are:

a. Hoop stress ($\sigma_{\emptyset}$): circumferential stress due to internal pressure.
b. Radial stress (σ_r): stress perpendicular to the longitudinal axis.
c. Axial stress (σ_a): along the length of the pipe.

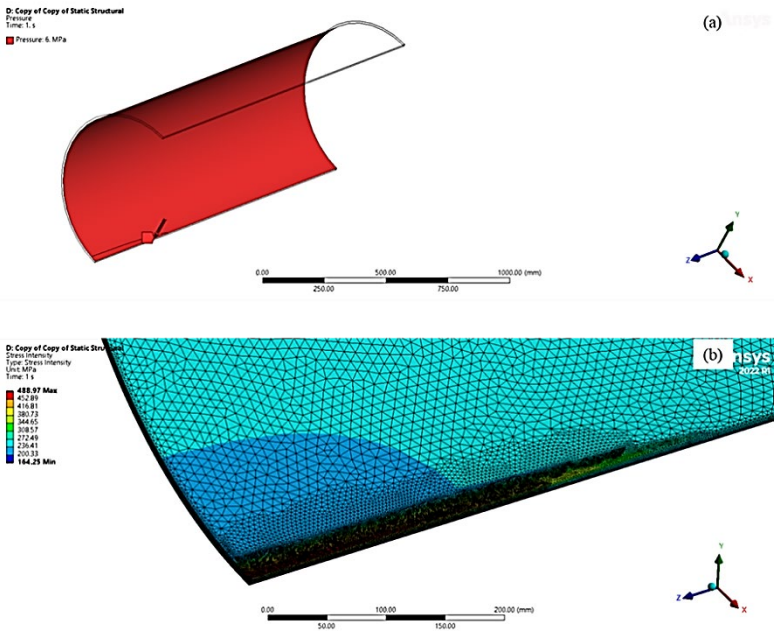

Fig. 6. Pipe specimen having internal corrosion defect depth of 1.7 mm, length of 454 mm, and width of 30 mm showing (a) internal pressure and (b) localized view of stress intensity at the vicinity of the internal defect

The radial displacement of the thick pipe subjected to pressure and temperature is provided by Eqs. (8-9), respectively:

$$\frac{d^2u_r}{dr^2}+\frac{1}{u}\frac{du_r}{dr}-\frac{1}{r^2}u_r=0 \tag{8}$$

$$\frac{d^2u_r}{dr^2}+\frac{1}{r}\frac{du_r}{dr}-\frac{u_r}{r^2}=\frac{1+\upsilon}{1-\upsilon}\alpha\frac{dt}{dr} \tag{9}$$

The general solution of the above differential Eqs. (10-11) provided the general solution for radial and hoop stress in thick-pipe in radial and tangential direction (Kljuno & Torlak, 2021; Sherbakov, 2011).

$$\sigma_r=\underbrace{\left[\frac{p_1r_1^2-p_2r_2^2}{r_2^2-r_1^2}-\frac{(p_1-p_2)r_1^2r_2^2}{r_2^2-r_1^2}\frac{1}{r^2}\right]}_{hydrostatic}+\underbrace{\left[\frac{E_1\alpha\Delta T}{2(1-\upsilon)}\frac{1}{lnk_{r12}}\left\{-lnk_{r2}-\frac{k_{r12}^2}{1-k_{12}^2}\left(1-\frac{1}{k_{r2}^2}\right)lnk_{r12}\right\}\right]}_{thermal} \tag{10}$$

$$\sigma_\emptyset=\underbrace{\left[\frac{p_1r_1^2-p_2r_2^2}{r_2^2-r_1^2}+\frac{(p_1-p_2)r_1^2r_2^2}{r_2^2-r_1^2}\frac{1}{r^2}\right]}_{hydrostatic}+\underbrace{\left[\frac{E_1\alpha\Delta T}{2(1-\upsilon)}\frac{1}{lnk_{r12}}\left\{-1-lnk_{r2}-\frac{k_{r12}^2}{1-k_{12}^2}\left(1+\frac{1}{k_{r2}^2}\right)lnk_{r12}\right\}\right]}_{thermal} \tag{11}$$

The first term of the above Equations defines the state of stresses due to pressure and the second term is due to the temperature difference between the inner and outer walls of the thick pipe. The above Equation was further simplified by applying boundary conditions for current studies:

Boundaries conditions:

a. At, $r=r_1$; internal pressure on the pipe was p_i (say p)
b. At, $r=r_2$; external pressure on the pipe was $p_{ext.}$=0
c. The variation of temperature (ΔT) = 0; the ΔT across the pipe wall (in the radial direction) and along the wall (axial direction) was null. In other words, the temperature gradient was non-existent in the present work. It means the second term in Equations 10 and 11 becomes zero.
d. The wall friction and all non-conservative forces were neglected; hence the axial stress σ_{axial} along the axial of the tube pipe (longitudinal stresses) is considered zero; it replicates the plane stress condition.

Therefore, the simplified form of Eqs. (10-11) are:

$$\frac{\sigma_r}{p}=\frac{1}{k_{r2}^2}\left[\frac{k_{r12}^2}{1-k_{r12}^2}-1\right], \tag{12}$$

$$\frac{\sigma_\emptyset}{p}=\frac{1}{k_{r2}^2}\left[\frac{k_{r12}^2}{1-k_{r12}^2}+1\right]. \tag{13}$$

The variation of σ_r and $\sigma_\emptyset$ with normalized radius are presented in **Fig. 7** and **Fig. 8** respectively. It was observed that it was $\sigma_\emptyset$ which induced along the circumference due to internal pressure and tries to increase pipeline diameter; the average diameter of the pipe was 711.2 mm which was much higher than the compared to thickness; hence it was $\sigma_\emptyset$ which resists the "bursting effect" due to internal pressure.

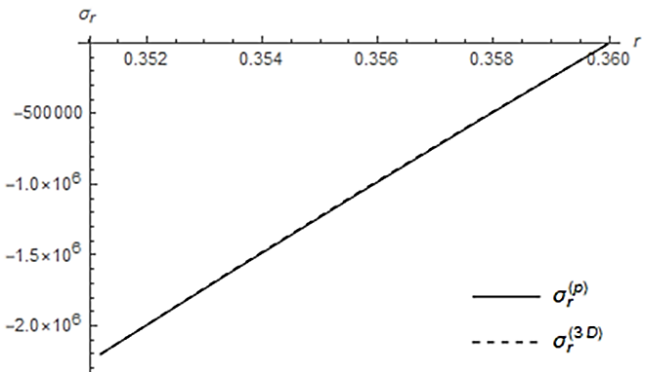

Fig. 7. The variation in radial stress with normalized radius

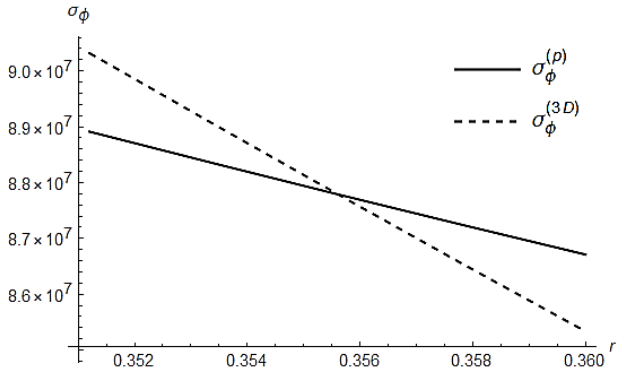

Fig. 8. The variation in hoop stress with normalized radius

3.3 Threshold Von-Mises stresses

The geometrical dimension of internal corrosion defect and corresponding maximum Von-Mises stress ($\sigma_{mises\ (max.)}$) at 3 different internal pressures of 2.2 MPa, 4.5 MPa, and 6 MPa are presented in **Tables 3-5**, respectively.

Table 3. Boundary condition for internal corrosion defects at an internal pressure of 2.2 MPa

Boundary condition no.	Length (z), mm	Width (x), mm	Depth (y), mm	Normalized depth	% increase in maximum σ_{mises}
1	30	26	0.5	0.06	5.41
2	30	26	0.9	0.10	13.54
3	30	26	1.7	0.19	30.72
4	30	62.1	0.5	0.06	0.51
5	30	62.1	0.9	0.10	9.38
6	30	62.1	1.7	0.19	13.41
7	30	134	0.5	0.06	0.00
8	30	134	0.9	0.10	1.57
9	30	134	1.7	0.19	6.82
10	157.4	26	0.5	0.06	12.82
11	157.4	26	0.9	0.10	28.42
12	157.4	26	1.7	0.19	65.48
13	157.4	62.1	0.5	0.06	8.34
14	157.4	62.1	0.9	0.10	23.69
15	157.4	62.1	1.7	0.19	40.84
16	157.4	134	0.5	0.06	4.05
17	157.4	134	0.9	0.10	11.81
18	157.4	134	1.7	0.19	29.25
19	454	26	0.5	0.06	15.11
20	454	26	0.9	0.10	33.22
21	454	26	1.7	0.19	78.36
22	454	62.1	0.5	0.06	12.31
23	454	62.1	0.9	0.10	27.40
24	454	62.1	1.7	0.19	63.26
25	454	134	0.5	0.06	7.48
26	454	134	0.9	0.10	18.35
27	454	134	1.7	0.19	43.73

Table 4. Boundary condition for internal corrosion defects at an internal pressure of 4.5 MPa

Boundary condition no.	Length (z), mm	Width (x), mm	Depth (y), mm	Normalized depth	% increase in maximum σ_{mises}
1	30	26	0.5	0.06	115.62
2	30	26	0.9	0.10	132.24
3	30	26	1.7	0.19	167.37
4	30	62.1	0.5	0.06	105.60
5	30	62.1	0.9	0.10	123.74
6	30	62.1	1.7	0.19	131.98
7	30	134	0.5	0.06	104.55
8	30	134	0.9	0.10	107.76
9	30	134	1.7	0.19	118.50
10	157.4	26	0.5	0.06	130.76
11	157.4	26	0.9	0.10	162.68
12	157.4	26	1.7	0.19	238.48
13	157.4	62.1	0.5	0.06	121.61
14	157.4	62.1	0.9	0.10	153.01
15	157.4	62.1	1.7	0.19	188.07
16	157.4	134	0.5	0.06	112.83
17	157.4	134	0.9	0.10	128.69
18	157.4	134	1.7	0.19	164.38
19	454	26	0.5	0.06	135.45
20	454	26	0.9	0.10	172.50
21	454	26	1.7	0.19	264.83
22	454	62.1	0.5	0.06	129.73
23	454	62.1	0.9	0.10	160.59
24	454	62.1	1.7	0.19	233.93
25	454	134	0.5	0.06	119.85
26	454	134	0.9	0.10	142.07
27	454	134	1.7	0.19	193.99

The boundary conditions for threshold Von-Mises stress, $\sigma_{mises|_{threshold}}$ were calculated using fatigue limit, yield strength, flow stress, and ultimate tensile strength of the pipeline steel. The maximum Von-Mises stresses were also addressed for corresponding internal pressure P_i.

Table 5. Boundary condition for internal corrosion defects at an internal pressure of 6 MPa.

Boundary condition no.	Length (z), mm	Width (x), mm	Depth (y), mm	Depth/thickness	% increase in maximum σ_{mises}
1	30	26	0.5	0.06	187.49
2	30	26	0.9	0.10	209.66
3	30	26	1.7	0.19	256.50
4	30	62.1	0.5	0.06	174.13
5	30	62.1	0.9	0.10	198.32
6	30	62.1	1.7	0.19	209.31
7	30	134	0.5	0.06	172.73
8	30	134	0.9	0.10	177.02
9	30	134	1.7	0.19	191.34
10	157.4	26	0.5	0.06	207.69
11	157.4	26	0.9	0.10	250.24
12	157.4	26	1.7	0.19	351.31
13	157.4	62.1	0.5	0.06	195.48
14	157.4	62.1	0.9	0.10	237.35
15	157.4	62.1	1.7	0.19	284.10
16	157.4	134	0.5	0.06	183.78
17	157.4	134	0.9	0.10	204.92
18	157.4	134	1.7	0.19	252.51
19	454	26	0.5	0.06	213.93
20	454	26	0.9	0.10	263.34
21	454	26	1.7	0.19	386.43
22	454	62.1	0.5	0.06	206.31
23	454	62.1	0.9	0.10	247.45
24	454	62.1	1.7	0.19	345.24
25	454	134	0.5	0.06	193.13
26	454	134	0.9	0.10	222.76
27	454	134	1.7	0.19	291.99

3.3.1 Design based on fatigue limit/ endurance limit

The engineering stress-engineering strain and true stress-true strain curve for structural steel considering elastic-plastic materials properties based on the Ramberg-Osgood Equation is shown in **Fig. 9** (Niesłony et al., 2008).

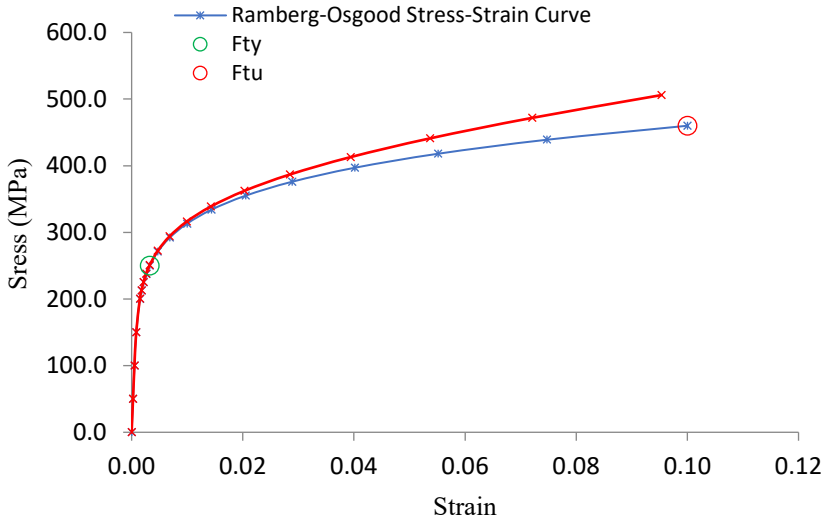

Fig. 9. True stress-true strain curve for pipeline steel. Fty and Ftu represent yield and ultimate tensile strength.

Van Aken et al. (2001) reported that fatigue limit (or endurance limit) is the optimum stress under which the steel could endure an infinite number of cycles (N); in other words, the material cannot fail despite any number of N. They reported that the fatigue limit (S_e) was one-half of the ultimate tensile strength σ_{UTS}. However, this relationship was valid up to σ_{UTS} of 1034 MPa which is within the range of our current studies.

The relationship between fatigue limit and ultimate tensile strength for pipeline steel is given as (Bannantine et al., 1990):

$$S_e = 0.5 \times \sigma_{UTS} \tag{14}$$

Therefore, the S_e for the material under consideration was 230 MPa which was well below the elastic yield strength (250 MPa) of the material. This stress was considered as the threshold stress below which the pipeline cannot fail for a given boundary condition. The internal corrosion defect influences the design stress of pipeline steel; hence the calculation of threshold boundary condition for such internal corrosion defect was made for all three internal pressures.

The boundary condition for an internal corrosion defect was defined by 4 parameters length (z), width (x), depth (y), and internal pressure (P_i). The generalized process parameters for σ_{mises} are defined in the form below:

$$\sigma_{mises} = f\{z, x, y, P_i\}. \tag{15}$$

When P_i = 2.2 MPa; the x, y, and z boundary conditions for all 27 cases provided a safe design. In other words, the domain for safe design considering threshold Von-Mises stress was:

$$\sigma_{mises|_{threshold}} = f\left[\{z_{min.}, z_{max.}\}\{x_{min.}, x_{max.}\}\{y_{min.}, y_{min.}\}\{0, 2.2\}\right] \tag{16}$$

when P_i raised to 4.5 MPa;

The type of Von-Mises stress was either minimum, threshold, or maximum dependent on the different boundary conditions. The FEM modelling provided the condition of σ_{mises} for different boundary conditions as:

$$\sigma_{mises|_{min.}} = f\{30, 134, 0.5, 4.5\} = 192.2\ MPa \tag{17}$$

$$\sigma_{mises|_{threshold}} = f\{30, 62.1, 1.7, 4.5\} = 217.99\ MPa < S_e \tag{18}$$

$$\sigma_{mises|_{max.}} = f\{454, 26, 1.7, 4.5\} = 342.8\ MPa > S_e \tag{19}$$

The threshold Von-Mises stress of 217.99 MPa was obtained at the boundary condition of $f\{30, 62.1, 1.7, 4.5\}$ while considering the design based on the fatigue limit of the pipeline steel. This process parameter provided the condition for safe design; in other words, for $f\{30, 62.1, 1.7, and\ 4.5\}$, the pipeline did not fail despite an infinite number of loading cycles. However, at P_i of 4.5 MPa, the $\sigma_{mises|_{max.}}$ was obtained as 342.8 MPa which was well above the yield strength of the material. Hence, at $f\{454, 26, 1.7, 4.5\}$, the material overcomes the elastic limit and envisages the elastic-plastic state; still, it did not fail (complete rapture) but deformed permanently. The pipeline can still carry the fluids without leaking and hence a "break-before-leak FEM model" was developed. Thus, it is suggested that at $f\{30, 62.1, 1.7, 4.5\}$ the pipeline did not require maintenance and can transport the fluids comfortably; however, at $f\{454, 26, 1.7, 4.5\}$ the pipeline may require maintenance considering the “break before leak” model. The threshold factor of safety ($FOS_{threshold}$) considering fatigue limit was calculated as:

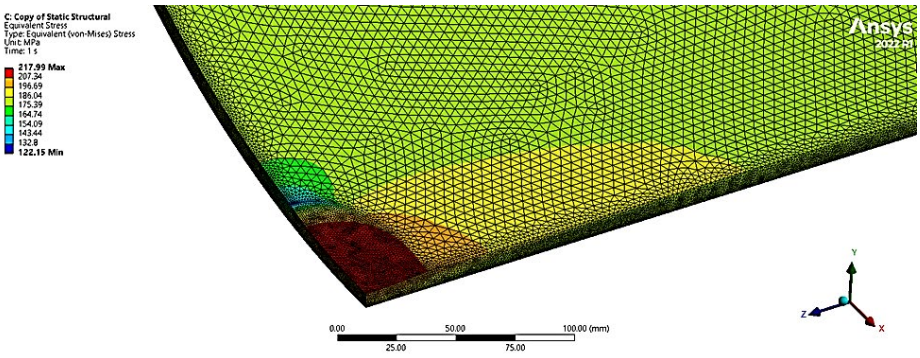

Fig. 10. $\sigma_{mises|_{threshold}}$ of 217.99 MPa at boundary condition $f\{30, 62.1, 1.7, 4.5\}$.

$$FOS_{threshold} = \frac{S_e}{\sigma_{mises|_{threshold}}} = 1.05 \tag{20}$$

It was interesting to note that the similar σ_{mises} was obtained at $f\{454, 26, 0.5, 4.5\}$ of 221.3 MPa, $f\{30, 26, 0.9, 4.5\}$ of 218.2 MPa, and $f\{30, 62.1, 1.7, 4.5\}$ of 218 MPa. It is suggested that the similarity in σ_{mises} for different defect dimensions was due to the “equivalent sharpness of defect geometry” based on linear-elastic fracture mechanics (Anderson & Anderson, 2005). The stress concentration in the vicinity of the defect depended not only on the defect dimension but also on the sharpness of the defect geometry. Considering all four process parameters, the generalized form of allowable boundary condition was defined below:

$$\sigma_{mises|_{allowable\ at\ x_{min.}}} = f\left[\{z_{min.}, z_{max.}\}\{y_{min.}, 0.9\}\{0, 4.5\}\right] \tag{21}$$

When the internal pressure in pipes is raised to 6 MPa, the specimen envisages σ_{mises} higher than S_e for all 27 boundary conditions. Therefore, in the context of all three internal pressures (2.2 MPa, 4.5 MPa, and 6 MPa); the generalized form of allowable σ_{mises} is provided below:

$$\sigma_{mises|_{allowable}} = f\ [\{z_{min.}, z_{max.}\}\{0, x_{min.}\}\{y_{min.}, 0.9\}\{0, 4.5\}] \tag{22}$$

3.3.2 Design based on yield strength of pipeline steel

The yield strength (σ_{ys}) for the material under investigation was 250 MPa. It is the highest stress that the pipeline steel can tolerate before permanent deformation (Gere & Timoshenko, 1997). It was above the S_e (230 MPa) of the material. This design hypothesis was still a "break-before-leak" model. When P_i = 2.2 MPa; the x, y, and z boundary conditions for all 27 cases provided a safe design. In other words, the boundary condition for safe design considering threshold Von-Mises stress was:

$$\sigma_{mises|_{threshold}} = f\ [\{z_{min.}, z_{max.}\}\{x_{min.}, x_{max.}\}\{y_{min.}, y_{min.}\}\{0, 2.2\}] \tag{23}$$

The above boundary conditions for $\sigma_{mises|_{threshold}}$ were in good agreement at P_i = 2.2 MPa for all design hypotheses considering failure stress greater than σ_{ys}. Hence, from here onwards this condition will be the same for further discussion.

However, when P_i increases to 4.5 MPa,

$$\sigma_{mises|_{min.}} = f\ \{30, 134, 0.5, 4.5\} = 192.2 \text{ MPa} \tag{24}$$

$$\sigma_{mises|_{threshold}} = f\ \{157.4, 134, 1.7, 4.5\} = 248.4 \text{ MPa} < \sigma_{ys} \tag{25}$$

The $\sigma_{mises|_{threshold}}$ is shown in **Fig. 11**.

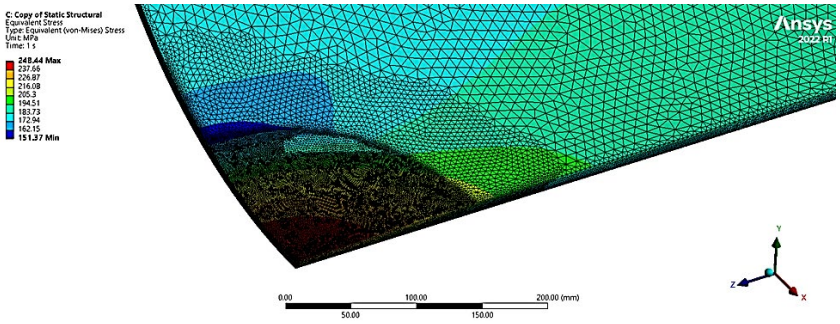

Fig. 11. $\sigma_{mises|_{threshold}}$ of 248.44 MPa at boundary condition $f\ \{157.4, 134, 1.7, 4.5\}$.

$$\sigma_{mises|_{max.}} = f\ \{454, 26, 1.7, 4.5\} = 342.8 \text{ MPa} > \sigma_{ys} \tag{26}$$

However, at the maximum P_i of 6 MPa; The σ_{mises} was above σ_{ys} for all conditions. Therefore, in the context of all three internal pressures (2.2 MPa, 4.5 MPa, and 6 MPa); the generalized form of allowable σ_{mises} is provided below:

$$\sigma_{mises|_{allowable}} = f\ [\{z_{min.}, 157.4\}\{x_{min.}, 134\}\{y_{min.}, 1.7\}\{0, 4.5\}] \tag{27}$$

The threshold factor of safety (*FOS*) considering the yield strength of the material was calculated as:

$$FOS_{threshold} = \frac{\sigma_{ys}}{\sigma_{mises|_{threshold}}} = 1.006. \tag{28}$$

Similar threshold boundary conditions for defects were also observed at $f\ \{157.4, 26, 0.9, 4.5\}$ of 246.8 MPa and $f\ \{454, 62.1, 0.9, 4.5\}$ of 244.9 MPa due to the "equivalent sharpness of defect geometry" based on linear-elastic fracture mechanics (Anderson & Anderson, 2005).

3.3.3 Design based on flow stress of pipeline steel

The instantaneous stress required to continue the plastic deformation, that is flow stress (σ_{flow}) is important for the safe design of the pipeline considering the elastic-plastic state. It envisages the plastic regime before the ultimate tensile stress (σ_{uts}). The Eq. (7) was used to calculate σ_{flow} and provided a quantitative value of 318.95 MPa.

When the P_i was 4.5 MPa,

$$\sigma_{mises|_{threshold}} = f\ \{157.4, 26, 1.7, 4.5\} = 318.07 \text{ MPa} < \sigma_{flow} \tag{29}$$

However, when P_i raised to 6 MPa,

$$\sigma_{mises|_{threshold}} = f\{157.4, 62.1, 0.9, 6\} = 317.01 \text{ MPa} < \sigma_{flow} \quad (30)$$

The $\sigma_{mises|_{threshold}}$ at internal pressure of 4.5 MPa and 6 MPa is shown in **Figs. (12-13)**, respectively.

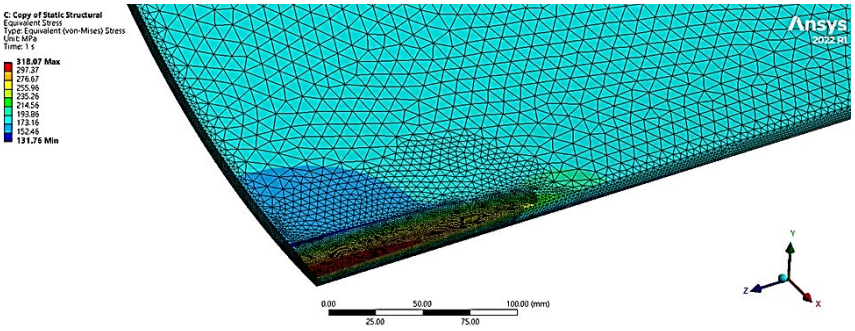

Fig. 12. $\sigma_{mises|_{threshold}}$ of 318.07 MPa at boundary condition $f\{157.4, 26, 1.7, 4.5\}$.

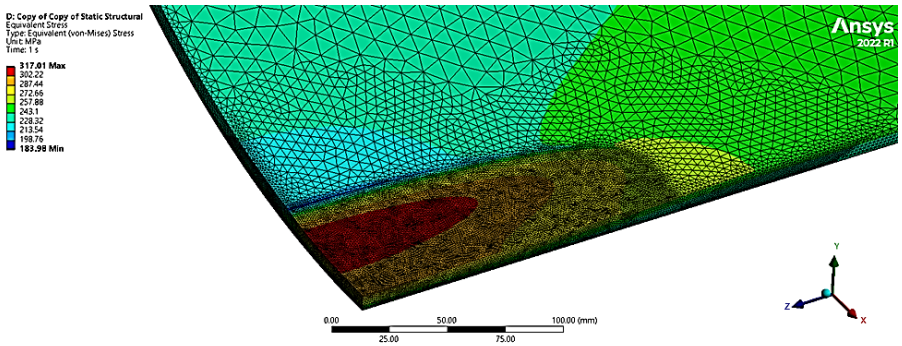

Fig. 13. $\sigma_{mises|_{threshold}}$ of 317.01 MPa at boundary condition $f\{157.4, 62.1, 0.9, 6\}$.

and,

$$\sigma_{mises|_{max.}} = f\{454, 26, 1.7, 6\} = 342.8 \text{ MPa} > \sigma_{flow} \quad (31)$$

Therefore, in the context of all three internal pressures (2.2 MPa, 4.5 MPa, and 6 MPa); the generalized form of allowable σ_{mises} is provided below:

$$\sigma_{mises|_{allowable}} = f\left[\{z_{min.}, 157.4\}\{0, 62.1\}\{y_{min.}, 1.7\}\{0, 6\}\right] \quad (32)$$

The threshold factor of safety (FOS) considering the flow stress of material was calculated as:

$$FOS_{threshold} = \frac{\sigma_{flow}}{\sigma_{mises|_{threshold}}} = 1.002 \quad (33)$$

3.3.4 Design based on ultimate tensile stress of pipeline steel

The σ_{uts} is 460 MPa for the material; It was interesting to note that there was only one boundary condition that provided the threshold value (457.1 MPa) which was also at the highest applied internal pressure of 6 MPa as shown in **Fig. 14.**

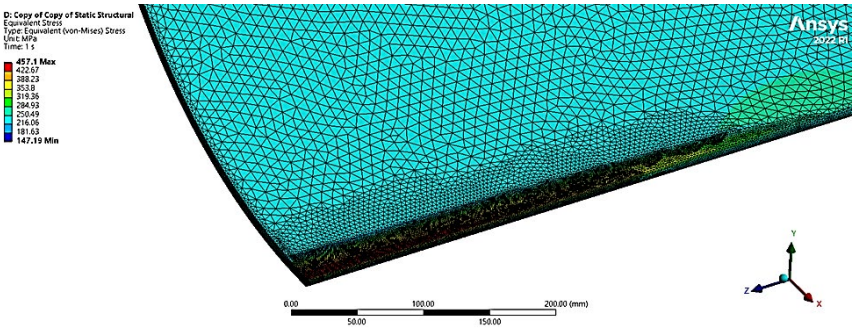

Fig. 14. $\sigma_{mises|_{threshold}}$ of 457.1 MPa at boundary condition $f\{454, 26, 1.7, 6\}$.

Hence,

$$\sigma_{mises|_{threshold}} = f\{454, 26, 1.7, 6\} = 457.1 \text{ MPa} < \sigma_{uts} \tag{34}$$

Hence, considering all three internal pressures:

$$\sigma_{mises|_{allowable}} = f\left[\{z_{min.}, z_{max.}\}\{0, x_{min.}\}\{y_{min.}, y_{max.}\}\{P_{i_{min.}}, P_{i_{max.}}\}\right] \tag{35}$$

It is suggested that the above boundary condition provided the largest possible defect with the sharpest geometry and highest stress concentration. This is the only model which provided a "leak-before-break" model instead of "break-before-leak". The pipeline requires immediate corrosion prevention under these circumstances. The all other extended geometrical dimensions for internal corrosion defects beyond the allowable limit, the pipeline envisages a complete rapture, and leakage of oil from the pipeline occurs with time.

$$FOS_{threshold} = \frac{\sigma_{uts}}{\sigma_{mises|_{threshold}}} = 1.006 \tag{36}$$

3.4 Stress intensity distribution at the threshold boundary condition

The $\sigma_{mises|_{threshold}}$ was obtained in the vicinity of internal corrosion defects; which means the pipeline was susceptible to failure at these localized positions. However, the σ_{mises} at other parts of the pipeline (complementary to internal corrosion defects) did not reach the failure pressure and design stress. It is suggested that the rise in σ_{mises} was due to the increase in stress intensity (K) because of geometrical sharpness and inequality of stress distribution (between the interface of the defect and the rest of the pipeline section) of internal corrosion defects which intensified the localized σ_{mises} (Anderson & Anderson, 2005). However, it has to be verified from K-distribution at threshold stress conditions. This hypothesis was studied by calculating K-distribution at the same boundary condition at which the $\sigma_{mises|_{threshold}}$ was obtained considering fatigue limit, yield stress, flow stress, and ultimate tensile stress of the material (Maiti, 2015; Suresh, 1998).

The K-distribution was obtained for threshold boundary conditions described in Eq. (18), Eq. (25), Eq. (30), and Eq. (34) of section 3.3 and shown in **Figs. 15-18**, respectively.

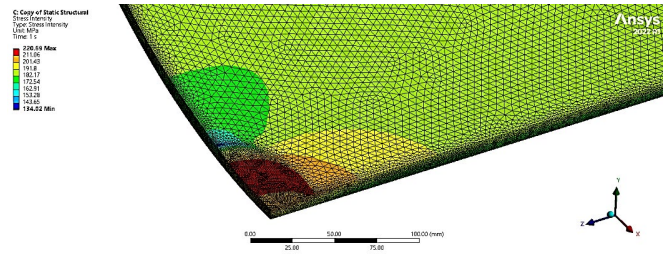

Fig. 15. K-distribution at boundary condition $f\{30, 62.1, 1.7, 4.5\}$.

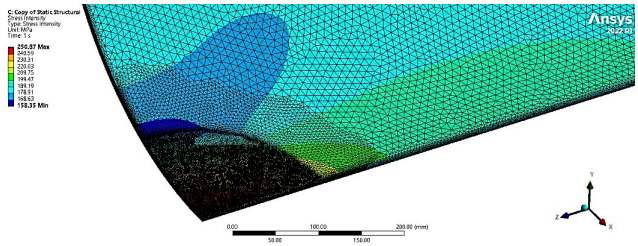

Fig. 16. K-distribution at boundary condition at boundary condition $f\{157.4, 134, 1.7, 4.5\}$.

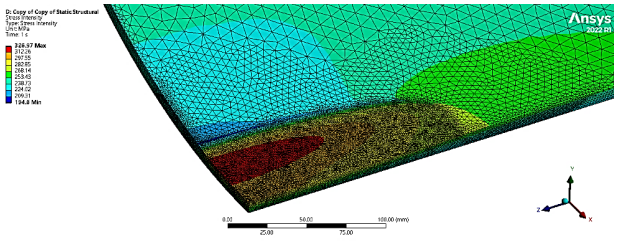

Fig. 17. K-distribution at boundary condition at boundary condition $f\{157.4, 62.1, 0.9, 6\}$.

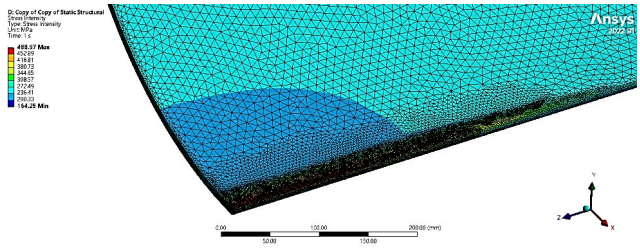

Fig. 18. K-distribution at boundary condition at boundary condition $f\{454, 26, 1.7, 6\}$.

It was interesting to observe that the lowest K-distribution (indicated by the dark blue colour) was obtained just outside the interface of internal corrosion defect geometry. It is suggested that the σ_{mises} accumulation inside the internal corrosion defect increases the K-distribution inside the internal corrosion defect geometry vis-à-vis lowers the K-distribution just outside of the internal corrosion defect. This inequality at the interface of internal corrosion defect envisages the pipeline to behave as the "specimen under tension-compression state". It raises localized stress induced near the vicinity of internal corrosion defect; once the threshold value of σ_{mises} is obtained then the pipeline becomes susceptible to failure under internal pressure. Any stress higher than the threshold leads to failure of the pipeline considering either the "leak before break" or "break before leak" hypothesis.

The K at threshold boundary condition was lowest (220.69 MPa) considering fatigue limit and highest (488.97 MPa) considering ultimate tensile strength as design criteria. Hence it is suggested that the optimum K after which the pipeline envisages complete rupture was 488.97 MPa. Any extended depth of internal corrosion defect and/or rise in internal pressure leads to the failure of the pipeline.

4. Discussion

The defect-free specimen exhibited a $P_{limit\ (FEM)}$ of 11.5 MPa and $P_{limit\ (theoretical)}$ of 11. 77 MPa. However, $P_{faliure\ (theoretical)}$ of 6.38 MPa and $P_{faliure\ (FEA)}$ of 6 MPa was obtained at the threshold boundary condition $f\ \{454, 26, 1.7, 6\}$. The agreement in these two parameters validated the hypothesis of applying internal corrosion defect by considering one-quarter of the pipe curvature. The effect of internal corrosion defect reduces the failure pressure to 52.17 %. Therefore, the oil-pumping capacity was reduced once an internal corrosion defect was induced in the pipeline. During the services, these internal corrosion defects grow and reach the threshold value reported in the current work. It is suggested that the pipe can be still operational if the working pressure has been less than $P_{faliure\ (FEA)}$ for threshold internal corrosion defect geometry $f\ \{454, 26, 1.7\}$. This threshold value provides a "normalized defect depth" (ratio of the depth of internal corrosion defect to the thickness of the pipeline) of 0.193. Any defect having a "normalized defect depth" value less than 0.193 provides a safe operation considering other process parameters adopted in the current work.

The analytical solutions for radial and hoop stress for pipelines with internal corrosion defects envisage the variation in $\sigma_{\emptyset}$ was prominent as compared to σ_r. Therefore, it was $\sigma_{\emptyset}$ which reduces the burst pressure for pipelines having an internal corrosion defect. Earlier studies also reported that the hoop stress was much higher than radial stress in thick pipelines. The σ_r influences the deformation (or strain) in the wall thickness of the pipeline, here the wall thickness of 8.8 mm was much less as compared to other dimensions of the pipeline which diminishes the material's ability to resist the failure pressure. On the other hand, $\sigma_{\emptyset}$ induced along the circumference due to internal pressure and tried to increase pipeline diameter, the average diameter of the pipe was 711.2 mm which was much higher than as compared to thickness; hence it was $\sigma_{\emptyset}$ which resists the bursting effect due to internal pressure. It is also important to understand the relationship between σ_{mises} and stress intensity (K). The relationship was obtained at the threshold boundary conditions reported in section 3.3 of the current work and depicted in **Fig. 19**.

From **Fig. 19**, the goodness of fit obtained was 0.99 which is within the acceptable limits for a linear curve fitting. The relation between maximum K and σ_{mises} is given below:

$$K = 1.1282 \times (\sigma_{mises}) - 28.002. \tag{37}$$

It is suggested that the above two curve fitting constants representing slope and intercept may depend upon the dimension of the internal corrosion defect, the dimension of the pipeline, and its material's property. This relationship can be studied further in future work. The distribution of σ_{mises} and K at the vicinity of the interface of internal corrosion defect provides an idea about higher inequality. The inequality in the distribution of these two parameters envisages the pipeline into a tension-compression situation. This situation replicates the effect of internal corrosion geometry on the 3-dimensional state of stress-strain. Therefore, it is suggested that not only the geometrical area of the internal corrosion defect affected the threshold condition but also the sharpness of the interface between corroded and uncorroded areas. The value of the factor of safety (FOS) is shown in Figure 20 at the threshold boundary condition. The design stress considered here was σ_{uts}.

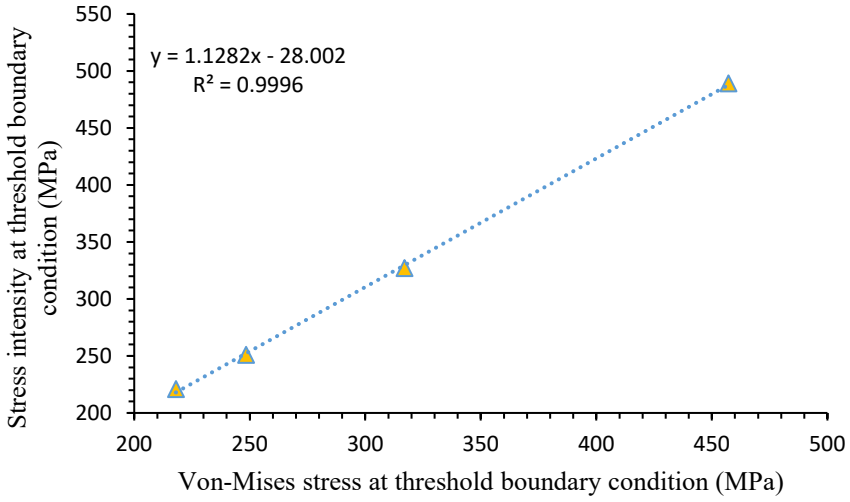

Fig. 19. Relationship between stress intensity and Von-Mises stress at threshold boundary condition.

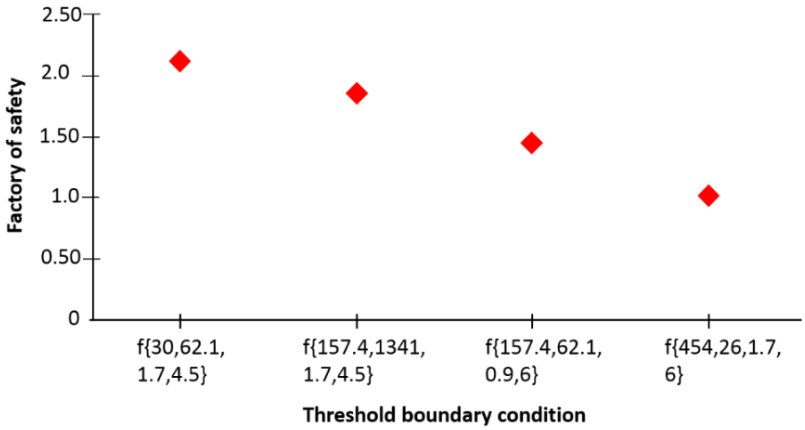

Fig. 20. FOS at threshold boundary condition.

The largest FOS of 2.11 was obtained at the threshold boundary condition considering fatigue limit as the optimum stress. The FOS decreases at the state of "elasticity" to "elastic-plastic" and then to the "complete plastic" state. It is then suggested that the FOS for the "break-before-leak" leak model can be anywhere between 2.11 to 1.45 and the pipeline cannot burst to rapture for these FOS. However, after, an FOS of 1.45, the pipeline overcomes flow stresses; after a rise of further stress intensity, these pipelines undergo a state of complete plasticity and a "leak-before-break" complete rupture has been occurred.

In the current work, the temperature gradient (ΔT) was considered null; it is suggested that the proposed FEA model can be studied considering both ΔT and Δp. Then the thermal constraints of the analytical equation for σ_r and $\sigma_\emptyset$ may come into consideration and threshold boundary conditions may be changed. A comparative study can be done and a more comprehensive FEA can be developed. The other process variables like oil friction (which provides axial stresses) can also be considered in future work.

5. Conclusion

The principal premises of the current work yield significant results which are concluded as:

1. The failure pressure of the uncorroded pipe ($P_{limit\ (FEA)}$) was 11.5 MPa. In contrast, for pipe with internal corrosion defect having the largest defect (1.7 mm), largest length (454 mm), and sharpest geometry (width of 30 mm), $P_{faliure\ (FEA)}$ was 6 MPa. The remaining strength at this boundary condition was 0.521.
2. The threshold boundary condition was f {30, 62.1, 1.7, 4.5}, f {157.4, 1341, 1.7, 4.5}, f {157.4, 62.1, 0.9, 6}, f {454, 26, 1.7, 6} considering fatigue limit, yield strength, flow stress, and ultimate tensile strength of the material, respectively.
3. The $\sigma_{mises|_{allowable}}$ was$f\ [\{z_{min.}, z_{max.}\}\{0, x_{min.}\}\{y_{min.}, 0.9\}\{0, 4.5\}]$, $f\ [\{z_{min.}, 157.4\}\{x_{min.}, 134\}\{y_{min.}, 1.7\}\{0, 4.5\}]$, $f\ [\{z_{min.}, 157.4\}\{0, 62.1\}\{y_{min.}, 1.7\}\{0, 6\}]$, $f\ \left[\{z_{min.}, z_{max.}\}\{0, x_{min.}\}\{y_{min.}, y_{max.}\}\{P_{i_{min.}}, P_{i_{max.}}\}\right]$ considering fatigue limit, yield strength, flow stress, and ultimate tensile strength of the material, respectively.
4. The lowest K distribution was obtained just outside the interface of internal corrosion defect geometry. The σ_{mises} accumulation inside the internal corrosion defect increases the K-distribution inside the internal corrosion defect geometry vis-à-vis lowers the K-distribution just outside of the internal corrosion defect. This inequality at the interface of internal corrosion defect envisages the pipeline to behave as the "specimen under tension-compression state". It raises localized stress induced near the vicinity of internal corrosion defect and once the threshold value of σ_{mises} is obtained then the pipeline becomes susceptible to failure under internal pressure. The variation in stress intensity with σ_{mises} showed a linear nature.
5. The σ_r influences the deformation (or strain) in the wall thickness of the pipeline, the wall thickness of 8.8 mm was much less as compared to other dimensions of the pipeline which diminishes the material's ability to resist the failure pressure. On the other hand, $\sigma_\emptyset$ induced along the circumference due to internal pressure and tries to increase pipeline diameter, the average diameter of the pipe was 711.2 mm which was much higher than to thickness; hence it was $\sigma_\emptyset$ which resists the "bursting effect" due to internal pressure.
6. The largest FOS of 2.11 was obtained at the threshold boundary condition considering fatigue limit as the optimum stress. The FOS decreases at the state of "elasticity" to "elastic-plastic" and then to the "complete plastic" state. It is then suggested that the FOS for the "break-before-leak" leak model can be anywhere between 2.11 to 1.45 and hence the pipeline cannot burst into rapture. However, after, an FOS of 1.45, the pipeline overcomes flow stresses and after a rise of further stress intensity, these pipelines undergo a state of complete plasticity and a "leak-before-break" complete rupture has occurred.

Acknowledgments

The authors wish to acknowledge The State Scientific Institution Joint Institute of Mechanical Engineering of The National Academy of Sciences of Belarus.

Funding

This work was carried out with the support of The Belarusian Republican Foundation for Fundamental Research (project number: T23RNF-125) and The Russian Science Foundation (grant number: 23-49-10061).

Conflicts of interest

The author declares no conflict of interest.

References

Aken, D. C. Van. (2001). Fatigue Endurance Limit of Steel. *Industrial Heating BNP Media, Inc*.

Alobaidi, W. M., Alkuam, E. A., Al-Rizzo, H. M., & Sandgren, E. (2015). Applications of ultrasonic techniques in oil and gas pipeline industries: A review. *American Journal of Operations Research*, *5*(04), 274.

Anderson, T. L., & Anderson, T. L. (2005). *Fracture Mechanics: Fundamentals and Applications, Third Edition*. Taylor & Francis.

Arumugam, T., Karuppanan, S., & Ovinis, M. (2020). Finite element analyses of corroded pipeline with single defect subjected to internal pressure and axial compressive stress. *Marine Structures*, *72*, 102746.

Branch, M., & Mahshahr, I. (2012). Use of polyurethane coating to prevent corrosion in oil and gas pipelines transfer. *International Journal of Innovation and Applied Studies*, *1*(2), 186-193.

Bannantine, J. A., Comer, J. J., & Handrock, J. L. (1990). *Fundamentals of Metal Fatigue Analysis*. Prentice Hall.

Benamor, A., Talkhan, A. G., Nasser, M., Hussein, I., & Okonkwo, P. C. (2018). Effect of temperature and fluid speed on the corrosion behavior of carbon steel pipeline in Qatari oilfield produced water. *Journal of Electroanalytical Chemistry*, *808*, 218–227.

Budhe, S., de Barros, S., & Banea, M. D. (2020). Prediction of the burst pressure for defective pipelines using different semi-empirical models. *Frattura Ed Integritá Strutturale*, *14*(52), 137–147.

Capula Colindres, S., Méndez, G. T., Velázquez, J. C., Cabrera-Sierra, R., & Angeles-Herrera, D. (2020). Effects of depth in external and internal corrosion defects on failure pressure predictions of oil and gas pipelines using finite element models. *Advances in Structural Engineering*, *23*(14), 3128–3139.

Dao, U., Sajid, Z., Khan, F., Zhang, Y., & Tran, T. (2023). Modeling and analysis of internal corrosion induced failure of oil and gas pipelines. *Reliability Engineering & System Safety*, *234*, 109170.

Dugstad, A., Lunde, L., & Nesic, S. (1994). Control of internal corrosion in multi-phase oil and gas pipelines. *Proceedings of the Conference Prevention of Pipeline Corrosion, Gulf Publishing Co*.

Folias, E. S. (1964). The stresses in a cylindrical shell containing an axial crack. *Report No. 64-174*.

Freire, J. L. F. (2024). Stress Analysis with Applications to Pipelines. In *Handbook of Pipeline Engineering* (pp. 1–32). Springer.

Gartland, P. O., Johnsen, R., & Ovstetun, I. (2003). Application of internal corrosion modeling in the risk assessment of pipelines. *NACE CORROSION*, NACE-03179.

Gere, J. M., & Timoshenko, S. (1997). *Mechanics of Materials*. PWS Publishing Company.

Godefroid, L. B., Sena, B. M., & Trindade Filho, V. B. da. (2017). Evaluation of microstructure and mechanical properties of seamless steel pipes API 5L type obtained by different processes of heat treatments. *Materials Research*, *20*(2), 514–522.

Han, C. J., Zhang, H., & Zhang, J. (2016). Failure pressure analysis of the pipe with inner corrosion defects by FEM. *International Journal of Electrochemical Science*, *11*(6), 5046–5062.

Hernandez-Rodriguez, M. A. L., Martinez-Delgado, D., Gonzalez, R., Unzueta, A. P., Mercado-Solís, R. D., & Rodriguez, J. (2007). Corrosive wear failure analysis in a natural gas pipeline. *Wear*, *263*(1–6), 567–571.

Hu, H., & Cheng, Y. F. (2016). Modeling by computational fluid dynamics simulation of pipeline corrosion in CO2-containing oil-water two phase flow. *Journal of Petroleum Science and Engineering*, *146*, 134–141.

Ijaola, A. O., Farayibi, P. K., & Asmatulu, E. (2020). Superhydrophobic coatings for steel pipeline protection in oil and gas industries: A comprehensive review. *Journal of Natural Gas Science and Engineering*, *83*, 103544.

Ilman, M. N. (2014). Analysis of internal corrosion in subsea oil pipeline. *Case Studies in Engineering Failure Analysis*, *2*(1), 1–8.

Kljuno, E., & Torlak, M. (2021). Pipe stress analysis using an analytical and a finite-volume method. *Advanced Technologies, Systems, and Applications V: Papers Selected by the Technical Sciences Division of the Bosnian-Herzegovinian American Academy of Arts and Sciences 2020*, 501–512.

Li, Q., Hu, H., & Cheng, Y. F. (2016). Corrosion of pipelines in CO2-saturated oil-water emulsion flow studied by electrochemical measurements and computational fluid dynamics modeling. *Journal of Petroleum Science and Engineering*, *147*, 408–415.

Lopez, M., Porcayo-Calderon, J., Casales-Diaz, M., Carrillo, I., Canto, J., de la Escalera, L. M. M., Cuevas-Arteaga, C., Regla, I., Melgoza-Aleman, R. M., & Martinez-Gomez, L. (2015). Internal corrosion solution for gathering production gas

pipelines involving palm oil amide based corrosion inhibitors. *International Journal of Electrochemical Science*, *10*(9), 7166–7179.

Maiti, S. K. (2015). *Fracture Mechanics*. Cambridge University Press.

Melchers, R. E. (2023). Internal corrosion of seabed 'parked'steel oil and gas pipelines. *Ocean Engineering*, *276*, 114145.

Moraes, N. R. D. C. de, Garcia, J. M., Baêta Júnior, E. de S., Cruz, R. B. da, & Brandao, L. P. (2021). Experimental and analytical investigation on the effect of heat treatment parameters on the mechanical properties of an API 5L X65 steel. *Materials Research*, *24*, e20200503.

Mousavi, S. S., & Moghaddam, A. S. (2020). Failure pressure estimation error for corroded pipeline using various revisions of ASME B31G. *Engineering Failure Analysis*, *109*, 104284.

Niesłony, A., Dsoki, C. el, Kaufmann, H., & Krug, P. (2008). New method for evaluation of the Manson–Coffin–Basquin and Ramberg–Osgood equations with respect to compatibility. *International Journal of Fatigue*, *30*(10), 1967–1977. https://doi.org/10.1016/j.ijfatigue.2008.01.012

Ossai, C. I., Boswell, B., & Davies, I. J. (2016a). Application of Markov modelling and Monte Carlo simulation technique in failure probability estimation—A consideration of corrosion defects of internally corroded pipelines. *Engineering Failure Analysis*, *68*, 159–171.

Ossai, C. I., Boswell, B., & Davies, I. J. (2016b). Stochastic modelling of perfect inspection and repair actions for leak–failure prone internal corroded pipelines. *Engineering Failure Analysis*, *60*, 40–56.

Poletskov, P., Gushchina, M., Polyakova, M., Alekseev, D., Nikitenko, O., Chukin, D., & Vasil'ev, Y. (2019). Development of alloyed pipe steel composition for oil and gas production in the Arctic region. *Resources*, *8*(2), 67.

Qin, G., & Cheng, Y. F. (2021). A review on defect assessment of pipelines: principles, numerical solutions, and applications. *International Journal of Pressure Vessels and Piping*, *191*, 104329.

Race, J., Oterkus, S., & Chang, E. (2020). A new methodology for the prediction of burst pressure for API 5L X grade flawless pipelines. *Ocean Engineering*, *212*, 107602.

Russell, T. W. F., Hodgson, G. W., & Govier, G. W. (1959). Horizontal pipeline flow of mixtures of oil and water. *The Canadian Journal of Chemical Engineering*, *37*(1), 9–17.

Sherbakov, S. (2011). Three-Dimensional Stress-Strain State of a Pipe with Corrosion Damage Under Complex Loading. In C.-H. Kuo (Ed.), *Tribology - Lubricants and Lubrication* (p. 332). IntechOpen. https://doi.org/10.5772/25114

Stalheim, D. G. (2005). The use of high temperature processing (HTP) steel for high strength oil and gas transmission pipeline applications. *Iron & Steel*, *40*(11), 699–704.

Sun, J., & Cheng, Y. F. (2018). Assessment by finite element modeling of the interaction of multiple corrosion defects and the effect on failure pressure of corroded pipelines. *Engineering Structures*, *165*, 278–286.

Sun, M., Chen, Y., Zhao, H., & Li, X. (2022). Analysis of the impact factor of burst capacity models for defect-free pipelines. *International Journal of Pressure Vessels and Piping*, *200*, 104805.

Suresh, S. (1998). *Fatigue of Materials*. Cambridge University Press.

Vanaei, H. R., Eslami, A., & Egbewande, A. (2017). A review on pipeline corrosion, in-line inspection (ILI), and corrosion growth rate models. *International Journal of Pressure Vessels and Piping*, *149*, 43–54.

Vishnuvardhan, S., Murthy, A. R., & Choudhary, A. (2023). A review on pipeline failures, defects in pipelines and their assessment and fatigue life prediction methods. *International Journal of Pressure Vessels and Piping*, *201*, 104853.

Wang, Z. M., & Zhang, J. (2016). Corrosion of multiphase flow pipelines: the impact of crude oil. *Corrosion Reviews*, *34*(1–2), 17–40.

Wang, Z., Zhou, Z., Xu, W., Yang, L., Zhang, B., & Li, Y. (2020). Study on inner corrosion behavior of high strength product oil pipelines. *Engineering Failure Analysis*, *115*, 104659.

Xu, L., & Cheng, Y. F. (2017). A finite element based model for prediction of corrosion defect growth on pipelines. *International Journal of Pressure Vessels and Piping*, *153*, 70–79.

Yang, W. (1980). *A generalized von Mises criterion for yield and fracture*.

Yang, Y., Liu, X., Yang, H., Fang, W., Chen, P., Li, R., Gao, H., & Zhang, H. (2022). A Semi Empirical Regression Model for Critical Dent Depth of Externally Corroded X65 Gas Pipeline. *Materials*, *15*(16), 5492.

Zhou, R., Gu, X., Bi, S., & Wang, J. (2022). Finite element analysis of the failure of high-strength steel pipelines containing group corrosion defects. *Engineering Failure Analysis*, *136*, 106203.